

Optimized 3D Gaussian Splatting using Coarse-to-Fine Image Frequency Modulation

Umar Farooq
University of Surrey
Guildford, United Kingdom
m.farooq@surrey.ac.uk

Jean-Yves Guillemaut
University of Surrey
Guildford, United Kingdom
j.guillemaut@surrey.ac.uk

Graham Thomas
University of Surrey
Guildford, United Kingdom
g.a.thomas@surrey.ac.uk

Adrian Hilton
University of Surrey
Guildford, United Kingdom
a.hilton@surrey.ac.uk

Marco Volino
University of Surrey
Guildford, United Kingdom
m.volino@surrey.ac.uk



Figure 1: Opti3DGS progressively grows levels to reduce redundant and unused Gaussians while maintaining accurate geometric structure and competitive quality.

Abstract

The field of Novel View Synthesis has been revolutionized by 3D Gaussian Splatting (3DGS), which enables high-quality scene reconstruction that can be rendered in real-time. 3DGS-based techniques typically suffer from high GPU memory and disk storage requirements which limits their practical application on consumer-grade devices. We propose Opti3DGS, a novel frequency-modulated coarse-to-fine optimization framework that aims to minimize the

number of Gaussian primitives used to represent a scene, thus reducing memory and storage demands. Opti3DGS leverages image frequency modulation, initially enforcing a coarse scene representation and progressively refining it by modulating frequency details in the training images. On the baseline 3DGS [Kerbl et al. 2023], we demonstrate an average reduction of 62% in Gaussians, a 40% reduction in the training GPU memory requirements and a 20% reduction in optimization time without sacrificing the visual quality. Furthermore, we show that our method integrates seamlessly with many 3DGS-based techniques [Fang and Wang 2024; Girish et al. 2024; Lee et al. 2024; Mallick et al. 2024; Papantonakis et al. 2024], consistently reducing the number of Gaussian primitives while maintaining, and often improving, visual quality.

Permission to make digital or hard copies of all or part of this work for personal or classroom use is granted without fee provided that copies are not made or distributed for profit or commercial advantage and that copies bear this notice and the full citation on the first page. Copyrights for components of this work owned by others than the author(s) must be honored. Abstracting with credit is permitted. To copy otherwise, or republish, to post on servers or to redistribute to lists, requires prior specific permission and/or a fee. Request permissions from permissions@acm.org.
CVMP '25, London, United Kingdom

© 2025 Copyright held by the owner/author(s). Publication rights licensed to ACM.
ACM ISBN 979-8-4007-2117-5/2025/12
<https://doi.org/10.1145/3756863.3769707>

CCS Concepts

• Computing methodologies → Computer graphics; Reconstruction.

Keywords

3D Gaussian Splatting, Efficient 3D Gaussian Splatting, Novel View Synthesis

ACM Reference Format:

Umar Farooq, Jean-Yves Guillemaut, Graham Thomas, Adrian Hilton, and Marco Volino. 2025. Optimized 3D Gaussian Splatting using Coarse-to-Fine Image Frequency Modulation. In *European Conference on Visual Media Production (CVMP '25), December 3–4, 2025, London, United Kingdom*. ACM, New York, NY, USA, 10 pages. <https://doi.org/10.1145/3756863.3769707>

1 Introduction

Photorealistic scene reconstruction remains a fundamental challenge in 3D computer vision, with applications spanning augmented and virtual reality, media production, and immersive gaming. Despite significant advancements, existing Novel View Synthesis (NVS) methods - particularly those based on Neural Radiance Fields (NeRF) [Mildenhall et al. 2021] - face substantial computational constraints [Deng and Tartaglione 2023; Hu et al. 2022; Li et al. 2023]. These constraints hinder broader adoption, especially on web, mobile, and edge devices, where efficient rendering and low memory usage are critical.

3D Gaussian Splatting (3DGS) [Kerbl et al. 2023], recently introduced as an explicit point-based NVS technique, achieves high visual fidelity with fast training and real-time rendering. However, it suffers from significant GPU memory and storage overhead [Niedermayr et al. 2024; Papantonakis et al. 2024], limiting its applicability across diverse device form factors.

To address these challenges we introduce Opti3DGS, a novel and efficient coarse-to-fine optimization strategy that reduces the number of Gaussians used to represent a scene. This translates into reduced memory and storage overheads compared to 3DGS [Kerbl et al. 2023]. Our approach begins with intentional over-reconstruction, which serves as an effective regularizer, followed by progressive refinement of the scene to balance detail and efficiency. Several techniques have been proposed which aim to reduce 3DGS memory and storage costs. Some focus on compressing the stored representation [Fan et al. 2024; Lee et al. 2024; Liu et al. 2024; Navaneet et al. 2023; Niedermayr et al. 2024], others optimize training speed and parallelization [Zhao et al. 2025], while a few attempt to minimize Gaussian primitive count during optimization itself [Lee et al. 2024; Papantonakis et al. 2024]. Our approach falls into the latter category, reducing Gaussian primitives during the optimization process, thereby decreasing GPU memory demands and accelerating training speed while maintaining visual quality. Notably, our method achieves these benefits as a plug-in approach without introducing additional learnable parameters or requiring lengthy optimizations.

Opti3DGS improves the baseline 3DGS [Kerbl et al. 2023], achieving a 62% reduction in Gaussian primitives, a 40% decrease in GPU memory usage during training, and a 20% speedup in optimization time. Our technique is highly modular and can be easily incorporated into most 3DGS-based pipelines with minimal modifications. Furthermore, we demonstrate its positive impact when integrated into optimized 3DGS variants such as MiniSplatting [Fang and Wang 2024] and Taming3DGS [Mallick et al. 2024], as well as other recent approaches [Girish et al. 2024; Lee et al. 2024; Papantonakis

et al. 2024]. Due to the coarse-to-fine nature of our approach, it naturally produces level-of-detail representation as a byproduct, shown in Figure 1, which could have useful applications in foveated rendering, streaming applications and advanced storage mechanisms. To summarize, our key contributions are:

- We present Opti3DGS, a framework to minimize the number of Gaussian primitives in a 3DGS scene resulting in improved training speed, memory and storage requirements.
- We propose a coarse-to-fine optimization strategy that increases the size of the Gaussians at the start of optimization and then slowly breaks down the large coarse Gaussians in a controlled fashion leading to an improved Gaussian densification process.
- We demonstrate that Opti3DGS can be seamlessly integrated into a wide range of existing 3DGS techniques minimizing the number of Gaussians used to represent the scene without sacrificing visual quality, and in most cases improving it.

2 Related Work

3DGS Compression: One approach to reduce the storage size of 3DGS scenes focuses on quantizing raw parameters stored for each Gaussian primitive [Fan et al. 2024; Lee et al. 2024; Liu et al. 2024; Navaneet et al. 2023; Niedermayr et al. 2024]. These enable efficient storage and transmission but since the optimization is done after 3DGS scene optimization, it does not lower GPU memory requirements during training and some of these methods require cumbersome decoding in GPU memory from a compressed representation which can be computationally expensive to render [Kim et al. 2024]. Some methods like [Girish et al. 2024] also include an efficient encoding and decoding mechanism for parameters during the optimization process, leading to both storage and compute time gains. However, in the case of [Girish et al. 2024] they introduce additional learnable parameters and use a separate neural network to decode the color values and face complications due to quantized vectors not being differentiable. [Girish et al. 2024] also use progressive resolution training which is different from our frequency based image filtering as outlined in section 4. A subset of these methods [Fang and Wang 2024; Girish et al. 2024; Niedermayr et al. 2024; Papantonakis et al. 2024; Wang et al. 2024] also compute the rendering importance of each Gaussian primitive based on its contribution to individual pixels, its relative size or the Gaussian neighborhood it is located in.

Gaussian Primitive Reduction: An alternative approach is to actively reduce the number of primitives during the optimization process [Fang and Wang 2024; Lee et al. 2024; Mallick et al. 2024; Papantonakis et al. 2024]. The Adaptive Density Control (ADC) mechanism in [Kerbl et al. 2023] removes Gaussians below a fixed opacity threshold at predefined intervals and densifies ones with large gradients by either splitting or cloning them. But despite these measures the primitive count increases rapidly and with much variation across runs [Mallick et al. 2024]. [Lee et al. 2024] proposed to learn a volume aware mask during training, incurring additional learnable parameters and optimization time, to remove primitives which are either small or have minimal contribution. But this approach is limited in its effectiveness because the problem stems

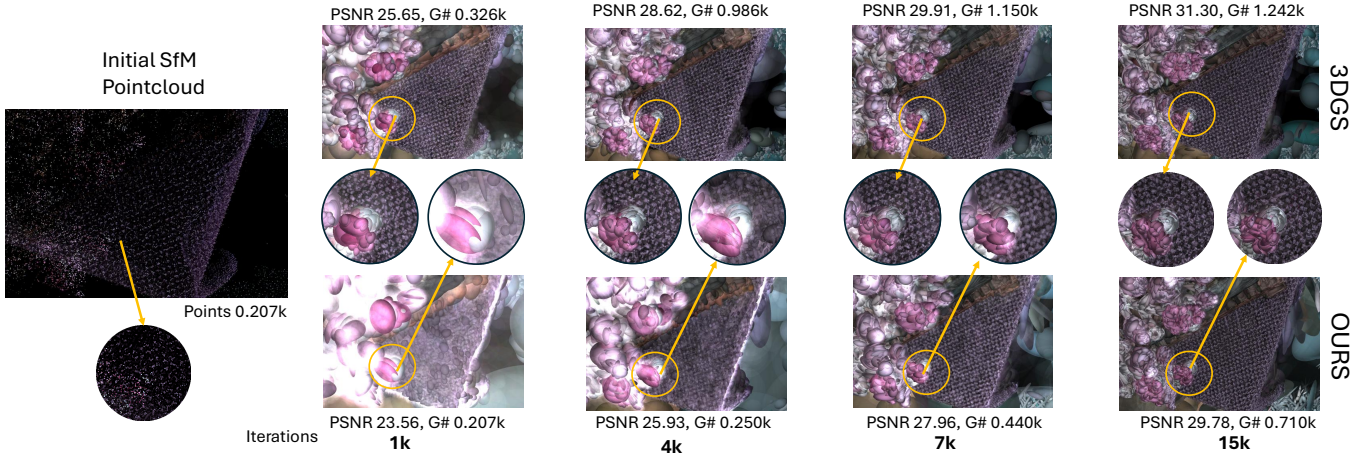


Figure 2: We start with uniform distribution of larger Gaussians as compared to 3DGS which starts heavy densification from the very start of optimization thus complicating the loss landscape. The zoomed views show efficient use of the initial sparse pointcloud by our approach.

from dense clustering of Gaussians in certain locations with a significant number of them not even contributing to the color at all [Fang and Wang 2024; Niedermayr et al. 2024]. [Fang and Wang 2024; Yang et al. 2025] show that there are multi-view inconsistencies between the centroids of the Gaussians and their location density is not uniform even in areas with uniform color and texture attributes and propose to regularize this inconsistency. [Papantonakis et al. 2024] prunes Gaussians during the optimization process based on their rendering importance and signs of local clustering, however they do not reduce the peak GPU memory requirements during the optimization process. [Mallick et al. 2024] propose the use of per-view per-pixel saliency maps to guide the densification process in a selective manner with predictable growth trend and used fused operations to speed up optimization. However all of these approaches require major changes in the ADC functionality and thus are not easily inter-compatible with each other and have unknown effects if combined. Whereas, Opti3DGS provides a plug-in approach that can be combined with various pipelines with almost no change to the core algorithm.

[Girish et al. 2024] also use a coarse-to-fine strategy but the downsize images in resolution progressively, in contrast Opti3DGS modulates the image frequency with the image resolution staying fixed. Both approaches have a distinct impact on the image pixels and quite different results. [Zhang et al. 2024] also use a frequency-based approach for optimizing 3DGS but they provide gradient signals in multiple separate frequency bands simultaneously with the goal of increasing visual quality which leads to a significantly higher Gaussian count.

Summary: We propose Opti3DGS, a coarse-to-fine frequency modulation approach to reduce the number of Gaussians by only changing the training images during the optimization process. Opti3DGS sits behind the ADC and is not directly involved in the differential rendering process and no changes need to be made in the core algorithm. This ensures wide ranging plug-in compatibility with most 3DGS based methods and also allows Opti3DGS to integrate with compression and quantization-based methods. Opti3DGS also

directly minimizes the Gaussians which leads to reduced GPU memory requirements during the optimization process reducing overall GPU memory requirements.

3 Method

3.1 Preliminaries: 3D Gaussian Splatting

3DGS [Kerbl et al. 2023] uses anisotropic Gaussians whose shape, color, opacity and refraction parameters are estimated via multi-view image-based optimization. Each Gaussian is defined by a covariance matrix Σ , a center position \mathbf{p} , opacity α , and spherical harmonics coefficients for color \mathbf{c} . The covariance matrix Σ is decomposed into a scaling matrix and a rotation matrix to facilitate differentiable optimization. For rendering, all Gaussians in the view frustum are splatted using onto a 2D plane followed by α -blending of the color based on Gaussian opacity to achieve the final image. The color C of a pixel is computed by blending N ordered 2D Gaussians that overlap the pixel, formulated as:

$$C = \sum_{i \in N} c_i \alpha_i \prod_{j=1}^{i-1} (1 - \alpha_j) \quad (1)$$

Here, the final color c_i of a pixel is defined by the color of each Gaussians, dependent on the spherical harmonics based on the view direction, falling on to the specific pixel multiplied by its individual opacity and the cumulative opacity α_i of the i Gaussians in front. This approach ensures that the contributions of overlapping Gaussians are blended accurately, resulting in a precise and realistic rendered image of the scene. The implementation also allows gradients to pass to an unrestricted number of Gaussians at any depth behind the camera position. Over the course of optimization, numerous tiny changes based on the gradients from differential rendering of multi-view images allow for the Gaussians to approximate shapes and colors close to real scene geometry.

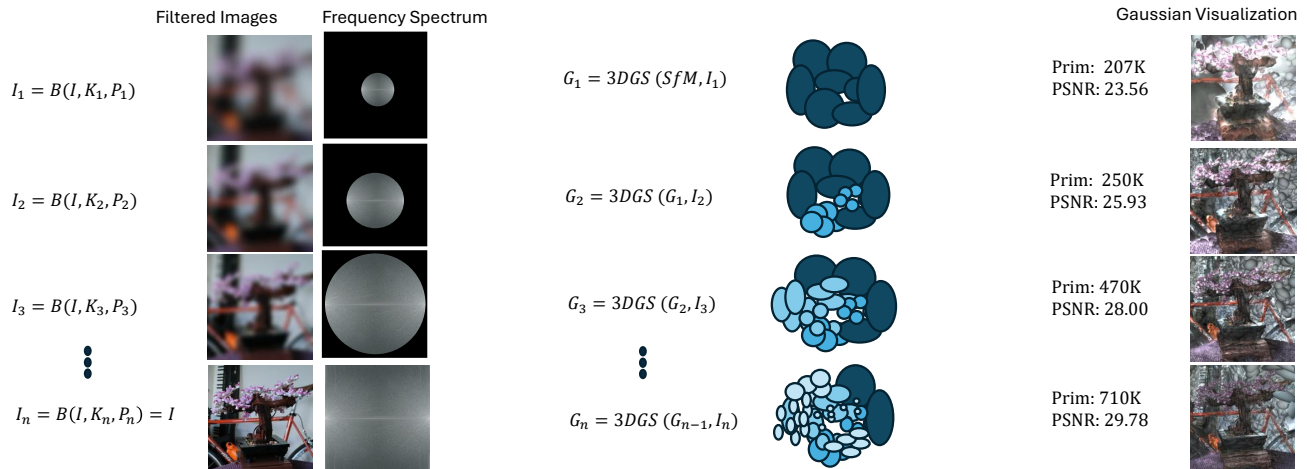


Figure 3: Method Overview: We start the optimization with very large and coarse Gaussians which are then densified based on the differentiable rendering signal. Specifically we control the frequency spectrum of the training images, gradually increasing the threshold for the low pass filtering.

3.2 Opti3DGS Overview

Our approach, shown in Figure 3, controls the frequency information in the training images which has a downstream effect on the ADC mechanism by providing it with a streamlined loss landscape. Starting with low frequency details in the scene, it steers the densification process to first approximate the large scale structure of the scene using large and coarse Gaussians, as shown in Figure 1. This also alleviates the pressure on the ADC to densify the image in regions with highly dense initial Structure-from-Motion (SfM) points, as shown in Figure 2. This indirect modulation signal allows the optimizer to approach a desirable balance between focusing on under and over-reconstructed regions of the scene.

3.3 Image Frequency Modulation

Digital images are made up of a spectrum of frequencies representing the structure and pattern of the color in them, with low frequencies corresponding to structure in the pixel space with gradual changes and high frequencies representing frequently changing color patterns like textures or white noise. There are a number of techniques for manipulating, enhancing or removing signals in different parts of the frequency spectrum depending on the downstream use-cases. Conceptually, a simple way of removing high frequency signals from an image exploits the local relation between pixels in a neighborhood to tease out only the consistent and stable color structures. The opposite can be thought to remove low frequency signals, but in practice a wide range of mathematical and statistical machinery is employed to perform various frequency restriction operations on images in an efficient fashion. Opti3DGS uses frequency manipulation on the training images as a tool to control the size of the Gaussians and deals with low pass filters, which only keep low frequencies or large scale structures while discarding high frequencies containing texture patterns and noise components. We experiment with mean, bi-lateral, Gaussian and Sobel filtering techniques in our approach and demonstrate

that mean filtering is the most effective, shown in Section 4.3. A simple low pass filtering operation on an image can be described as:

$$G[i, j] = \sum_{u=-k}^k \sum_{v=-k}^k H[u, v] F[i - u, j - v] \quad (2)$$

where H and F represent the convolutional kernel and the input image respectively with G being the resulting image from the operation. Importantly, we fix the stride to 1 for all our experiments and adjust the padding to ensure the spatial dimensions of the image don't change during any step of the image processing pipeline. The values in the filtering kernel in the context of a convolution operation define the type of filtering that will happen to the image. Gaussian kernels emphasize the central values in the filtering window of the image whereas a mean filter weighs them equally.

3.4 Frequency Training Schedule

Starting with very large coarse Gaussians and progressively adding high frequency details requires a schedule of frequency removal and addition. We explore various mechanisms, including linear, cosine, cosine restarting, exponential and step functions, as shown in Figure 4, which control the intensity of the image frequency modulation given the current training iteration as input. For the step function we define a single value for a fixed iteration interval and define all intervals accordingly. Based on ablation experiments, described in Section 4.3, the step function to be most effective.

3.5 Progressive Growing Pipeline

Opti3DGS employs a progressive frequency control strategy with five distinct image and scene quality levels I_n and G_n respectively in range $n = (1 - 5)$ as depicted in Fig.1. We start by first obtaining a sparse scene reconstruction and initial 3D points using SfM on the training images I and this initial sparse representation acts as

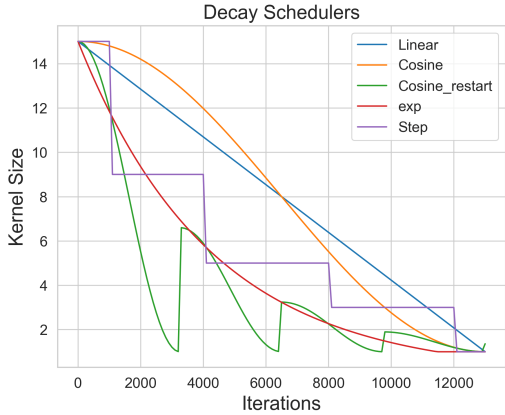


Figure 4: Visualization of different decay rates reported in our work. The vertical axis shows the current kernel size for the filtering algorithm for any given iteration. Note we stop all frequency modulation after 12,000 iterations and pass full sized images for the remaining 18,000 iterations.

our G_0 at $n = 0$ for initializing the Gaussians.

$$G_0 = SfM(I) \quad (3)$$

Then for each subsequent level in our coarse-to-fine optimization process we use the last set of Gaussians G_{n-1} as the starting point and the normal 3DGS optimization loss is used to optimize G_n using the filtered images I in range $n = (1 - 5)$.

$$G_n = 3DGS(G_{n-1}, I_n) \quad (4)$$

where the images I_n are obtained from the filtering function $B(I, K_n, P_n)$. For each level the images get progressively sharper and more high frequency content is allowed to remain in the image. For the last level, $n = 5$, we directly pass the original training images to the 3DGS optimizer.

$$G_5 = 3DGS(G_4, I) \quad (5)$$

For level-of-detail representation results, the model for any given level is saved at the last iteration before transitioning to the next level. The number of levels as well as the decay schedule can be easily changed for downstream applications.

4 Results and Evaluation

Datasets: We report results on the MipNeRF360 [Barron et al. 2022], DeepBlending [Hedman et al. 2021] and Tanks and Temples [Knapitsch et al. 2017] datasets with a total of 13 scenes which include a good mix of indoor and outdoor unbounded scenes, as well as scenes with low-frequency textures.

Implementation Details: All our ablations, graphs and results are reported as the average scores for all held-out test views averaged for all 13 scenes, with the exception of Figure 1 and Figure 6 which report the results averaged for all test views for the bicycle scene. For testing the impact of our module on top of other 3DGS based methods, we first reproduce the software environment and reported results from the authors and then re-run the code with our changes applied using the authors provided training and evaluation scripts for fair comparison and evaluation. We do not change any

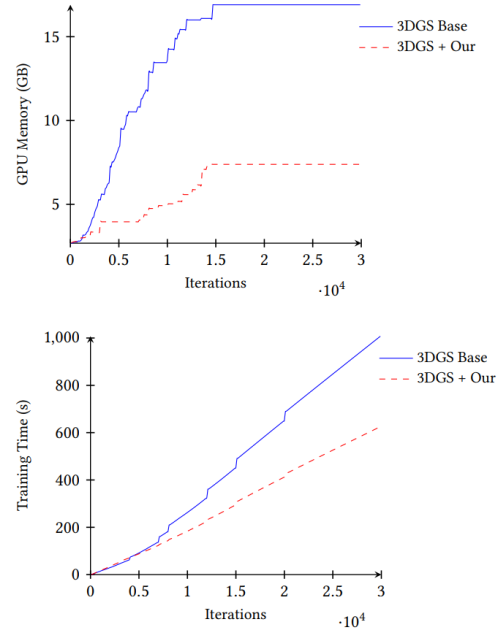


Figure 5: We reduce the GPU memory required during optimization due to a reduced Gaussian primitive load, which also reduces the total optimization time. These results are for 3DGS[Kerbl et al. 2023] across the bicycle scenes and are representative of all scenes tested.

hyper-parameters or settings for any of the methods except for 3DGS [Kerbl et al. 2023] where we change the *scaling_lr*= 0.01, *densification_interval*= 500 and *densify_grad_thresh*= 0.0001. All experiments and comparison were undertaken using a NVidia H200 GPU. We use the step decay function as shown in Figure 4 with a mean blur filter with an initial kernel size of 15 in all our experiments and stop frequency modulation after the first 12,000 iterations. Further ablations of these parameters are presented in Section 4.3. Reconstructed scene models and code to reproduce results will be made publicly available.

Metrics: We use PSNR, SSIM and LPIPS for quantitative evaluation and analysis of the trained models and for reproducing relevant baselines. We follow the established best practice of keeping every 8th frame for a hold-out test set and train all our experiments for 30,000 iterations and comply with the image resolution convention from [Kerbl et al. 2023] for using full scale images for DeepBlending [Hedman et al. 2021] and Tanks and Temples [Knapitsch et al. 2017] and using 2nd and 4th image resolution levels after Colmap processing for MipNeRF360 [Barron et al. 2022] indoor and outdoor scenes respectively.

4.1 Progressive Growing Impact

Our approach achieves excellent reduction in the number of Gaussians used to represent a scene while maintaining competitive visual quality or improving the visual quality.

Reduced Gaussian Footprint: We achieve a reduction in the number of Gaussians in all datasets for each of the methods as reported

Table 1: Opti3DGS consistently lowers Gaussian count for all reported methods as well as improving the reconstruction quality for some. Note we also report the maximum Gaussian count for methods where it peaks before the end of optimization. No optimization parameters were changed for any method except for 3DGS+Ours* as described in section 4.

Method	Deep Blending[Hedman et al. 2021]						Tanks & Temples[Knapitsch et al. 2017]						Mip-NeRF360[Barron et al. 2022]									
	SSIM ↑	PSNR ↑	LPIPS ↓	FPS ↑	Time (m:s) ↓	#G (10 ⁶) ↓	Peak #G ↓	SSIM ↑	PSNR ↑	LPIPS ↓	FPS ↑	Time (m:s) ↓	#G (10 ⁶) ↓	Peak #G ↓	SSIM ↑	PSNR ↑	LPIPS ↓	FPS ↑	Time (m:s) ↓	#G (10 ⁶) ↓	Peak #G ↓	
Compact3DGS[Lee et al. 2024]	0.904	29.79	0.254	274	15:41	1.052	1.428	0.834	23.34	0.199	150	10:33	0.839	1.006	0.799	27.01	0.242	275	16:53	1.489	2.400	-
Compact3DGS + Ours	0.904	29.81	0.258	348	13:46	0.831 (215)	1.130	0.827	23.26	0.217	218	08:31	0.601 (285)	0.718	0.792	26.96	0.262	357	13:37	1.048 (305)	1.794	-
Reduced-3DGS[Papantonakis et al. 2024]	0.903	29.63	0.248	420	11:00	0.925	-	0.841	23.52	0.186	258	06:45	0.568	-	0.810	27.29	0.229	408	11:55	1.460	-	-
Reduced-3DGS + Ours	0.904	29.76	0.251	558	09:53	0.697 (295)	-	0.834	23.52	0.203	352	05:38	0.409 (285)	-	0.801	27.14	0.250	560	09:55	1.061 (275)	-	-
Mini-Splatting[Fang and Wang 2024]	0.904	29.88	0.256	839	10:00	0.352	0.378	0.832	23.22	0.202	602	07:10	0.203	0.217	0.820	27.25	0.219	699	11:01	0.496	0.611	-
Mini-Splatting + Ours	0.908	30.01	0.254	849	10:07	0.344 (28)	0.376	0.834	23.17	0.204	614	07:13	0.197 (385)	0.211	0.821	27.26	0.219	711	11:21	0.488 (28)	0.610	-
Taming3DGS[Mallick et al. 2024] (budget)	0.899	29.75	0.273	1038	02:14	0.294	-	0.832	23.66	0.213	411	02:19	0.319	-	0.793	27.21	0.262	523	14:36	0.666	-	-
Taming3DGS (budget) + Ours	0.905	30.00	0.269	1036	02:22	0.294 (95)	-	0.834	23.90	0.215	431	02:17	0.318 (95)	-	0.788	27.27	0.274	593	14:11	0.5735 (145)	-	-
Taming3DGS[Mallick et al. 2024] (big)	0.909	30.04	0.233	326	06:15	3.593	-	0.859	24.14	0.160	107	05:04	2.290	-	0.823	27.82	0.207	228	06:46	3.251	-	-
Taming3DGS (big) + Ours	0.911	30.13	0.237	431	04:57	2.212 (385)	-	0.854	24.22	0.175	163	03:38	1.333 (425)	-	0.817	27.77	0.223	318	05:19	2.345 (285)	-	-
EAGLES[Girish et al. 2024]	0.91	29.86	0.25	247	11:22	1.19	-	0.84	23.27	0.20	379	06:19	0.65	-	0.81	27.23	0.24	274	09:40	1.33	-	-
EAGLES + Ours	0.91	29.86	0.25	304	11:36	0.87 (275)	-	0.83	23.28	0.21	417	07:00	0.58 (115)	-	0.79	26.90	0.27	329	13:21	0.90 (325)	-	-
3DGS[Kerbl et al. 2023]	0.900	29.54	0.247	293	11:34	2.795	-	0.844	23.69	0.178	108	07:19	1.825	-	0.813	27.53	0.221	247	11:42	3.157	-	-
3DGS + Ours*	0.902	29.56	0.255	611	10:26	0.953 (465)	-	0.823	23.15	0.217	258	05:56	0.658 (445)	-	0.809	27.09	0.237	308	09:50	1.327 (385)	-	-



(a) 3DGS* Error Map [PSNR: 25.20, Gaussians: 6,071,666]



(b) Ours Error Map [PSNR: 25.01, Gaussians: 2,107,227]

Figure 6: Pixel level comparison of error maps against the ground truth image. Our approach maintains similar quantitative scores while using fewer Gaussians and results in a decreased pixel wise error. Note the absence of noise like bright points in our results, due to the removal of tiny redundant Gaussians.

in Table 1, which is impressive given that all listed methods aim to reduce the file size and Gaussian count and are already extremely optimized to this end. Averaged across all reported methods for the three datasets, there is a drop of -0.03dB in PSNR for an average drop of 26% in the number of Gaussians. This represents a good trade-off with a -0.13dB PSNR drop for a 27% drop in #G for Mip-NeRF360, a +0.09dB PSNR gain for a 26% drop in #G for Deep Blending and a -0.05dB PSNR drop for a 25% drop in #G for Tanks&Temples. The single largest reported PSNR drop in Table

1. of 0.44dB equals a quality loss of 10% while reducing #G by 58% and train time by 16%.

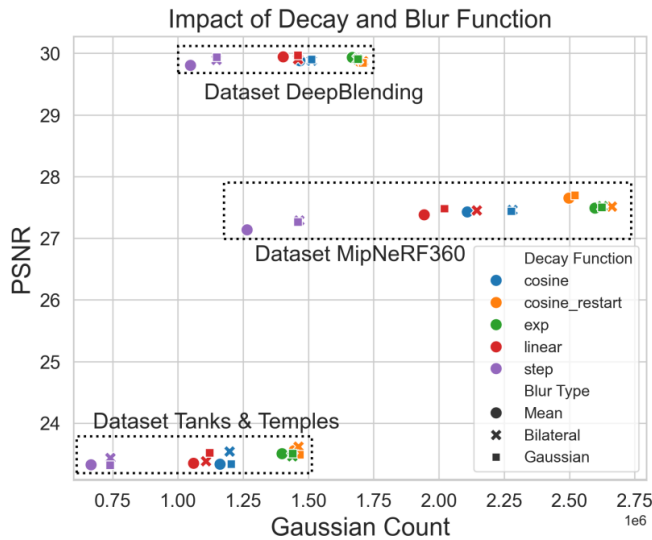
When applied on 3DGS[Kerbl et al. 2023], our method reduces the Gaussian count by up-to 62% as reported in Table 1.

Peak Gaussian Count: For some methods, such as MiniSplatting [Fang and Wang 2024] and Compact3DGS [Lee et al. 2024], the final Gaussian count is not a true representation of the GPU memory requirements as the Gaussian count peaks at various points during training. Opti3DGS also reduces the peak Gaussian load as well as the final Gaussian count for both MiniSplatting[Fang and Wang 2024] and Compact3DGS[Lee et al. 2024] as reported in Table 1.

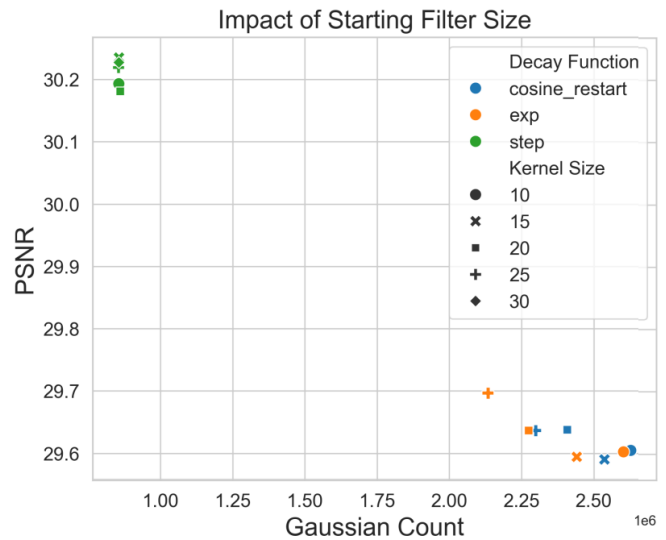
Reduced Optimization Time and GPU Memory: A reduction in the number of Gaussians during the optimization process also leads to accumulated speed-ups in terms of optimization time as reported in Table 1 with an illustrative example visualized in the Figure 5. For 3DGS[Kerbl et al. 2023], our method reduces the optimization time by 20% and the training GPU memory requirements by up-to 40%. Notably, the optimization time for EAGLES[Girish et al. 2024] and Taming3DGS[Mallick et al. 2024](budget) slightly increases, but this could potentially arise from other hyper-parameters in those methods being optimized for a different training regimes and having a high degree of coupling. Note, we do not change any parameters in any of these methods except for 3DGS. Still, the Gaussian footprint is reliably reduced. The GPU memory required for optimization also decreases proportionally to the reduction in the Gaussian count. An illustrative example of GPU memory reduction is highlighted in Figure 5.

Level-of-Detail Representation: Opti3DGS also produced different levels-of-details as a natural by-product of our progressive growing approach. We currently only store the last level-of-detail to save disk space. However, it allows a scene to be trained to the maximum level-of-detail before running out of available GPU memory. Figure. 5 and Figure 2 indicate this might be an useful feature and intermediate representations from Opti3DGS might be more useful than ones obtained naively from 3DGS. We leave further exploration of this idea as future work.

Performance on Scenes with Low Texture: Opti3DGS gives the highest gains in visual quality on DeepBlending where all scenes include large untextured walls and ceilings with the PSNR improving on all seven reported methods. There is a gain of +0.09dB in PSNR for a 26% drop in #G for Deep Blending and we leave further



(a) Impact of different decay rate functions.



(b) Impact of different initial kernel sizes.

Figure 7: Ablation Experiments: (a) shows the impact of using different decay rate functions to control the size of the kernel used for image filtering. Combining step decay function with the mean filter performs best and is adopted across all our experiments. Note each point is the average score for that respective dataset. (b) shows the impact of using different initial kernel sizes with the mean filter. Larger starting kernel size reduces the Gaussian count but the quality plateaus.

investigation of this result in context of the SfM induced bias to future work.

Table 2: Compares our progressive filtering approach to the progressive downsampling approach proposed by [Girish et al. 2024]. Both are applied on 3DGS[Kerbl et al. 2023] in isolation without any additional changes. We use the default image downsizing based approach with starting resize threshold of 0.3 and duration of 0.7 for [Girish et al. 2024]. Our progressive filtering uses the step decay function with mean blur filter and an initial kernel size of 15, which is consistent with the results reported in Table. 1. Results indicate that both approaches have a distinct impact on different datasets.

Dataset	Method	SSIM \uparrow	PSNR \uparrow	LPIPS \downarrow	#G (10^6) \downarrow
Mip-NeRF360	EAGLES[Girish et al. 2024]-Downsizing	0.810	27.44	0.232	2.412
	Ours-Filtering	0.808	27.37	0.238	2.195
Tanks & Temples	EAGLES[Girish et al. 2024]-Downsizing	0.843	23.59	0.191	1.090
	Ours-Filtering	0.843	23.71	0.191	1.229
Deep Blending	EAGLES[Girish et al. 2024]-Downsizing	0.904	29.55	0.247	2.325
	Ours-Filtering	0.906	29.68	0.246	2.118

4.2 Efficient use of Gaussian Primitives

For 3DGS [Kerbl et al. 2023] our approach reduces the Gaussian primitive count by up-to 62% but it also favours more efficient use of any given Gaussian budget, meaning it can derive more quality and a better reconstruction given the same number of Gaussian primitives. This explains the simultaneous increase of +0.09dB in Deep Blending dataset accompanied by a 26% drop in number of

Gaussians used. The ADC in 3DGS generally adds redundant and even wasteful Gaussians in some parts of the scene driving up the compute requirements with no gain in quality [Lee et al. 2024; Niedermayr et al. 2024; Papantonakis et al. 2024]. Our method reduces the wasteful and redundant use of Gaussians as well and drives the quality higher as shown by the lack of bright noise pattern seen in Figure 6.

4.3 Ablations

Modulation Schedule: We experiment with various frequency modulation schedules in Figure 4. The results indicate that the step schedule function works better than linear, exponential, or cosine variants across all scenes in the datasets by a significant margin. This is explained by the fact that it allows the ADC to optimize a fixed Gaussian budget rather than optimizing and simultaneously handling new insertions.

Blur Filter: We also test various types of image filtering algorithms including Gaussian, bilinear and mean filtering to determine the best approach. The results, shown in Figure 4, indicate that the mean filter performs well on most type of scenes. Surprisingly Gaussian and bilateral filtering perform poorly, possibly because they give more weight to the pixel at the center of the kernel or to edge information in the images.

Kernel Size: Holding the step function constant and using a mean filter, we perform experiments to evaluate the impact of the image filtering intensity on the final reconstruction quality. Results, shown in Figure 7, indicate that starting from a larger filter improves performance but the trend peaks quickly. We adopt the step

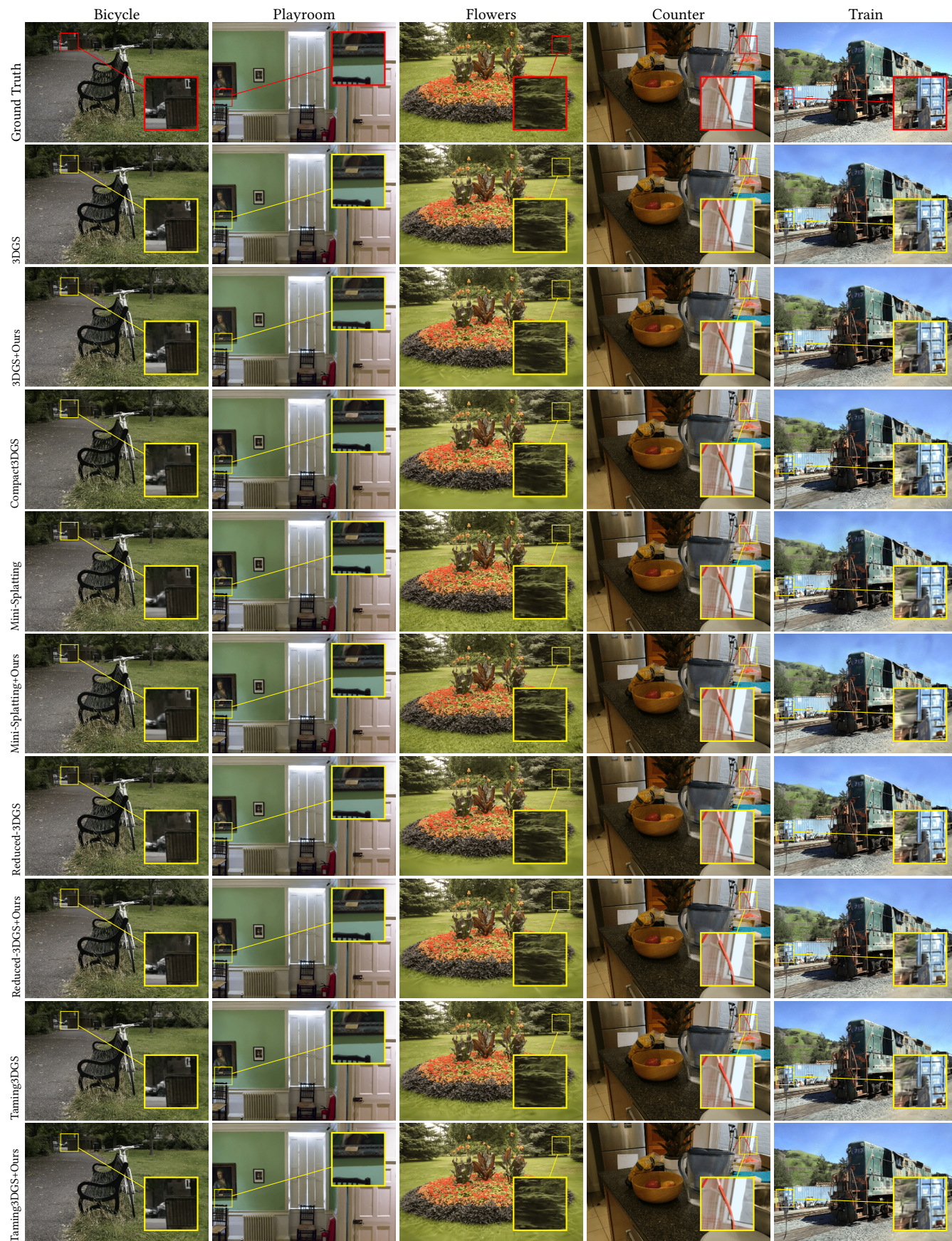


Figure 8: Qualitative results of Opti3DGS when integrated into different 3DGS-based methods with zoomed in cut-outs.

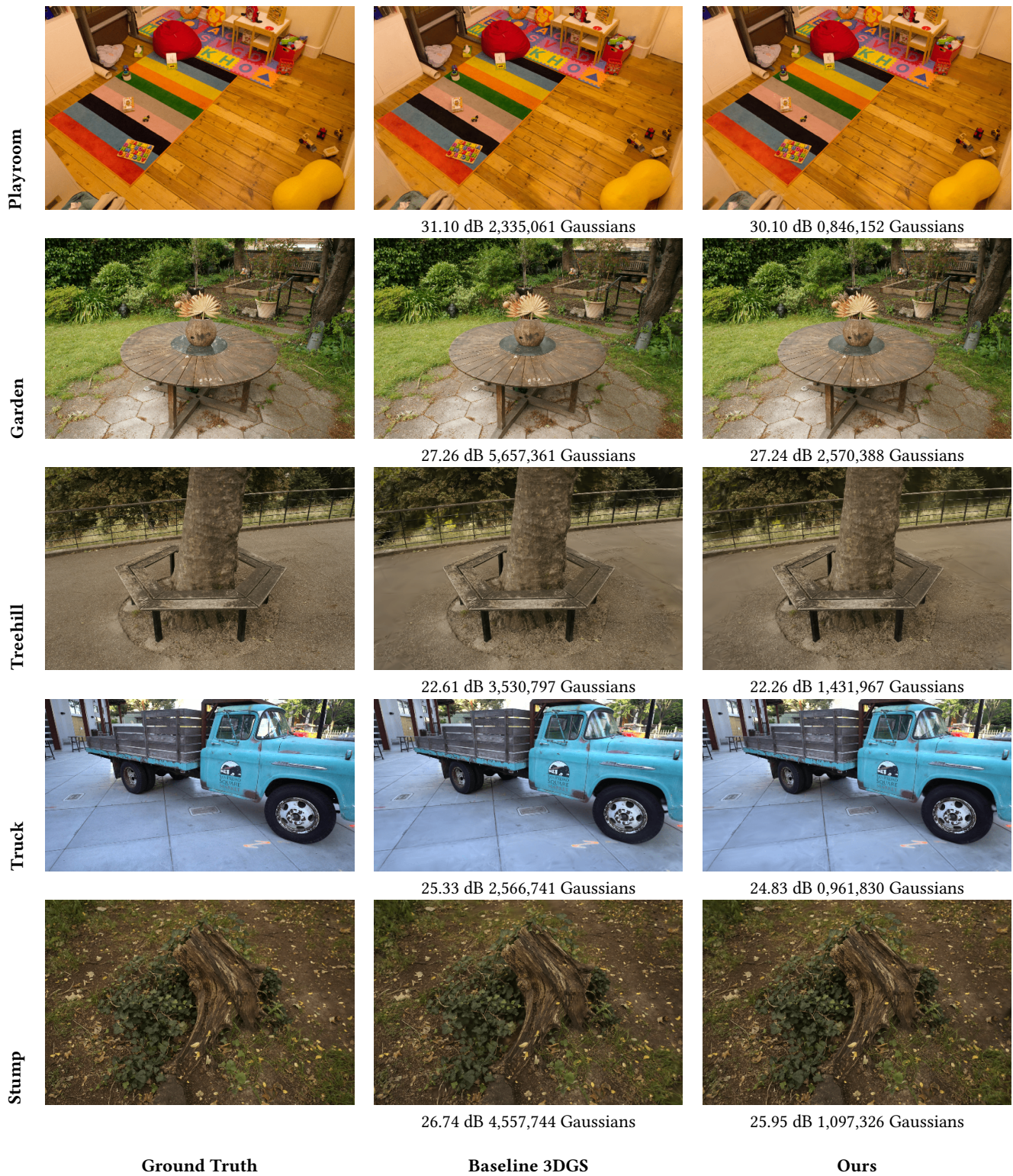


Figure 9: Comparison of our results with 3DGS and respective ground truths. Best viewed zoomed in.

decay function with an initial kernel size of 15 in all our experiments for the first 12,000 iterations.

Improvement over EAGLES: EAGLES focuses on storage size and render and train time, starts from 3DGS and uses: (i) MLP based quantization (SH color, opacity and rotation attributes); (ii) influence based Gaussian pruning; (iii) progressive resolution training. Opti3DGS only uses progressive frequency modulation and 3DGS+Opti3DGS when compared to the full highly optimized EAGLES pipeline achieves better average Gaussian count by 6.3%, better average Train Time by 4.2% and better average FPS by 43% while there is a minor average PSNR loss of 0.18 dB.

Full-EAGLES with Our Frequency Modulation: ‘EAGLES + Ours’ in Tab. 1 shows that our frequency modulation when plugged into the full EAGLES pipeline as a replacement for its progressive resolution downsampling improves average Gaussian count by 23% with an average PSNR drop of 0.1 dB. Slight loss in quality could be due to EAGLES hyperparameters being optimized for its own resolution modulation and we do not change any of them to ensure a fair and clean comparison.

Core Novelty comparison with EAGLES: EAGLES progressive training module gradually increases image resolution whereas Opti3DGS only modulates image frequency and when both are applied to 3DGS in isolation our frequency modulation shows a distinct and different impact from resolution downsampling. Our approach reduces Gaussian footprint for two of the three datasets as well as slightly improving the reconstruction quality for two datasets.

5 Conclusions

Summary: We have presented Opti3DGS, a simple yet highly effective framework that minimizes the number of Gaussian primitives in 3DGS-based pipelines. We demonstrated an average reduction of 62% in Gaussian count, a 40% reduction in the training GPU memory requirements and a 20% reduction in optimization time without sacrificing the visual quality compared to 3DGS [Kerbl et al. 2023]. We have conducted an extensive quantitative and qualitative evaluation that has shown Opti3DGS can be seamlessly integrated into a wide range of current 3DGS-based approaches resulting in a positive impact on primitive count in all cases. The contribution of Opti3DGS enables 3DGS-based pipelines and scene reconstructions to be more usable on a range of consumer-grade devices due to reduced primitives and therefore storage, transmission and utilization requirements making the technology more widely accessible.

Limitations: Currently Opti3DGS is agnostic to the image content and applies filtering on the entire training set uniformly, but it fails to take into account structural boundaries and large constant object which could be better represented by singular Gaussians with the right pixel level emphasis. A content-aware extension will be considered in the future.

Future Work will focus on using edge and depth aware image filtering operations and investigating the impact of using projected Gaussian centroid density in the image space to selectively guide attention to areas with lower visual variation which remain poorly densified by the ADC. We will also explore the extension of Opti3DGS to dynamic scenes exploiting the level-of-detail representation.

References

- Jonathan T. Barron, Ben Mildenhall, Dor Verbin, Pratul P. Srinivasan, and Peter Hedman. 2022. Mip-NeRF 360: Unbounded Anti-Aliased Neural Radiance Fields. *CVPR* (2022).
- Chenxi Lola Deng and Enzo Tartaglione. 2023. Compressing explicit voxel grid representations: fast nerfs become also small. In *Proceedings of the IEEE/CVF Winter Conference on Applications of Computer Vision*. 1236–1245.
- Zhiwen Fan, Kevin Wang, Kairun Wen, Zehao Zhu, DeJia Xu, and Zhangyang Wang. 2024. LightGaussian: Unbounded 3D Gaussian Compression with 15x Reduction and 200+ FPS. In *Advances in Neural Information Processing Systems*, A. Globerson, L. Mackey, D. Belgrave, A. Fan, U. Paquet, J. Tomczak, and C. Zhang (Eds.), Vol. 37. Curran Associates, Inc., 140138–140158.
- Guangchi Fang and Bing Wang. 2024. Mini-Splatting: Representing Scenes with a Constrained Number of Gaussians. In *Computer Vision – ECCV 2024: 18th European Conference, Milan, Italy, September 29–October 4, 2024, Proceedings, Part LXXVII* (Milan, Italy). Springer-Verlag, Berlin, Heidelberg, 165–181.
- Sharath Girish, Kamal Gupta, and Abhinav Shrivastava. 2024. Eagles: Efficient accelerated 3d gaussians with lightweight encodings. In *European Conference on Computer Vision*. Springer, 54–71.
- Peter Hedman, Pratul P. Srinivasan, Ben Mildenhall, Jonathan T. Barron, and Paul Debevec. 2021. Baking Neural Radiance Fields for Real-Time View Synthesis. *ICCV* (2021).
- Tao Hu, Shu Liu, Yilun Chen, Tiancheng Shen, and Jiaya Jia. 2022. Efficientnerf efficient neural radiance fields. In *Proceedings of the IEEE/CVF Conference on Computer Vision and Pattern Recognition*. 12902–12911.
- Bernhard Kerbl, Georgios Kopanas, Thomas Leimkühler, and George Drettakis. 2023. 3d gaussian splatting for real-time radiance field rendering. *ACM Transactions on Graphics* 42, 4 (2023), 1–14.
- Sieun Kim, Kyungjin Lee, and Youngki Lee. 2024. Color-cued Efficient Densification Method for 3D Gaussian Splatting. In *Proceedings of the IEEE/CVF Conference on Computer Vision and Pattern Recognition*. 775–783.
- Arno Knapitsch, Jaesik Park, Qian-Yi Zhou, and Vladlen Koltun. 2017. Tanks and Temples: Benchmarking Large-Scale Scene Reconstruction. *ACM Transactions on Graphics* 36, 4 (2017).
- Joo Chan Lee, Daniel Rho, Xiangyu Sun, Jong Hwan Ko, and Eunbyung Park. 2024. Compact 3D Gaussian Representation for Radiance Field. In *Proceedings of the IEEE/CVF Conference on Computer Vision and Pattern Recognition (CVPR)*. 21719–21728.
- Ruilong Li, Hang Gao, Matthew Tancik, and Angjoo Kanazawa. 2023. Nerfacc: Efficient sampling accelerates nerfs. In *Proceedings of the IEEE/CVF International Conference on Computer Vision*. 18537–18546.
- Xiangrui Liu, Xinju Wu, Pingping Zhang, Shiqi Wang, Zhu Li, and Sam Kwong. 2024. CompGS: Efficient 3D Scene Representation via Compressed Gaussian Splatting (*MM '24*). Association for Computing Machinery, New York, NY, USA, 2936–2944.
- Saswat Subhajiyo Mallick, Rahul Goel, Bernhard Kerbl, Markus Steinberger, Francisco Vicente Carrasco, and Fernando De La Torre. 2024. Taming 3dgs: High-quality radiance fields with limited resources. In *SIGGRAPH Asia 2024 Conference Papers*. 1–11.
- Ben Mildenhall, Pratul P. Srinivasan, Matthew Tancik, Jonathan T. Barron, Ravi Ramamoorthi, and Ren Ng. 2021. Nerf: Representing scenes as neural radiance fields for view synthesis. *Commun. ACM* 65, 1 (2021), 99–106.
- KL Navaneet, Kossar Pourahmadi Meibodi, Soroush Abbasi Koohpayegani, and Hamed Pirsiavash. 2023. Compact3d: Compressing gaussian splat radiance field models with vector quantization. *arXiv preprint arXiv:2311.18159* (2023).
- Simon Niedermayr, Josef Stumpfegger, and Rüdiger Westermann. 2024. Compressed 3D Gaussian Splatting for Accelerated Novel View Synthesis. In *Proceedings of the IEEE/CVF Conference on Computer Vision and Pattern Recognition (CVPR)*. 10349–10358.
- Panagiotis Papanotakis, Georgios Kopanas, Bernhard Kerbl, Alexandre Lanvin, and George Drettakis. 2024. Reducing the Memory Footprint of 3D Gaussian Splatting. *Proceedings of the ACM on Computer Graphics and Interactive Techniques* 7, 1 (2024), 1–17.
- Henan Wang, Hanxin Zhu, Tianyu He, Runsen Feng, Jiajun Deng, Jiang Bian, and Zhibo Chen. 2024. End-to-End Rate-Distortion Optimized 3D Gaussian Representation. In *European Conference on Computer Vision*.
- Haosen Yang, Chenhao Zhang, Wenqing Wang, Marco Volino, Adrian Hilton, Li Zhang, and Xiatao Zhu. 2025. Improving Gaussian Splatting with Localized Points Management. In *Proceedings of the IEEE Conference on Computer Vision and Pattern Recognition*.
- Jiahui Zhang, Fangneng Zhan, Muyu Xu, Shijian Lu, and Eric Xing. 2024. FreGS: 3D Gaussian Splatting with Progressive Frequency Regularization. In *2024 IEEE/CVF Conference on Computer Vision and Pattern Recognition (CVPR)*. 21424–21433.
- Hexu Zhao, Haoyang Weng, Daohan Lu, Ang Li, Jinyang Li, Aurojit Panda, and Saining Xie. 2025. On Scaling Up 3D Gaussian Splatting Training. In *International Conference on Representation Learning*, Y. Yue, A. Garg, N. Peng, F. Sha, and R. Yu (Eds.), Vol. 2025. 35642–35661.